

Emergence of SARS-CoV-2 escape mutations during Bamlanivimab therapy in a phase II randomized clinical trial

Received: 15 September 2021

Accepted: 19 September 2022

Published online: 26 October 2022

 Check for updates

A full list of authors and their affiliations appears at the end of the paper.

SARS-CoV-2 mutations that cause resistance to monoclonal antibody (mAb) therapy have been reported. However, it remains unclear whether in vivo emergence of SARS-CoV-2 resistance mutations alters viral replication dynamics or therapeutic efficacy in the immune-competent population. As part of the ACTIV-2/A5401 randomized clinical trial (NCT04518410), non-hospitalized participants with symptomatic SARS-CoV-2 infection were given bamlanivimab (700 mg or 7,000 mg) or placebo treatment. Here, we report that treatment-emergent resistance mutations [detected through targeted Spike (S) gene next-generation sequencing] were significantly more likely to be detected after bamlanivimab 700 mg treatment compared with the placebo group (7% of 111 vs 0% of 112 participants, $P = 0.003$). No treatment-emergent resistance mutations among the 48 participants who received 7,000 mg bamlanivimab were recorded. Participants in which emerging mAb resistant virus mutations were identified showed significantly higher pretreatment nasopharyngeal and anterior nasal viral loads. Daily respiratory tract viral sampling through study day 14 showed the dynamic nature of in vivo SARS-CoV-2 infection and indicated a rapid and sustained viral rebound after the emergence of resistance mutations. Participants with emerging bamlanivimab resistance often accumulated additional polymorphisms found in current variants of concern/interest that are associated with immune escape. These results highlight the potential for rapid emergence of resistance during mAb monotherapy treatment that results in prolonged high-level respiratory tract viral loads. Assessment of viral resistance should be prioritized during the development and clinical implementation of antiviral treatments for COVID-19.

Across a broad spectrum of viral infections, host immune pressure^{1,2} and antiviral therapy^{3–5} can select for viral escape mutations. The detection and characterization of antiviral resistance mutations have been critical for the selection of appropriate antiviral therapies and the advancement of our understanding of viral adaptation against evolutionary

pressures⁶. Monoclonal antibody (mAb) therapy has been one of key treatment options for non-hospitalized persons with early SARS-CoV-2 infections and mild to moderate COVID-19^{7,8}. Bamlanivimab was the first mAb to receive US Food and Drug Administration (FDA) emergency use authorization (EUA) after it was demonstrated that treatment with

✉ e-mail: davey@ucsd.edu; jli@bwh.harvard.edu

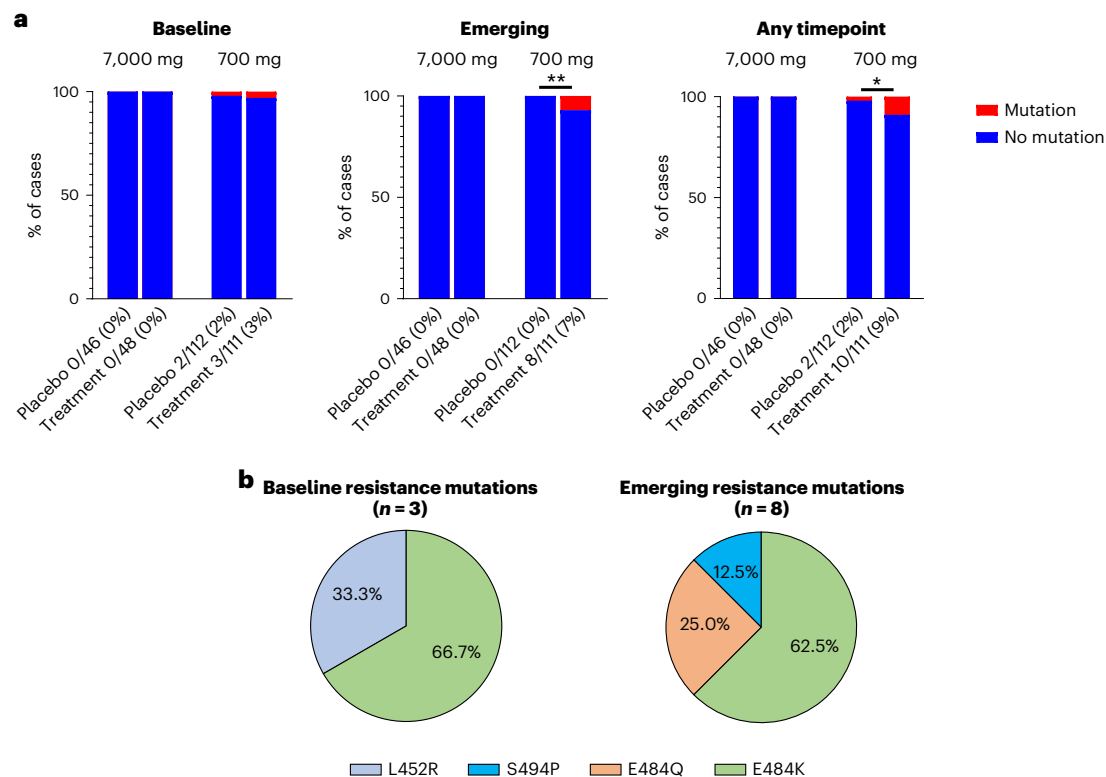


Fig. 1 | Prevalence of SARS-CoV-2 primary resistance mutations. a, Percent of participants harbouring primary resistance mutations L452R, E484K, E484Q, F490S and S494P at $\geq 20\%$ frequency in the bamlanivimab 7,000 mg and 700 mg treatment and placebo arms at baseline, emergent and at any timepoint. Participants without quantifiable viral load at baseline and/or follow-up

timepoints were grouped with those without resistance. *P* values were calculated using Fisher's exact test. **P* < 0.05, ***P* < 0.01. **b**, Pie charts showing distribution of baseline and emergent resistance mutations in the treatment arm. One participant had E484K at baseline with emerging E484Q mutation.

bamlanivimab decreased nasopharyngeal (NP) SARS-CoV-2 detection and the risk of hospitalization or death when compared to placebo⁹. The emergence of SARS-CoV-2 sequence changes was reported shortly after the introduction of mAbs^{7,10,11}, but there has not been definitive evidence that the emergence of SARS-CoV-2 resistance mutations can lead to altered in vivo intrahost viral replication dynamics and loss of therapeutic efficacy.

ACTIV-2/A5401 is a platform trial to evaluate the efficacy of antiviral agents to prevent disease progression in non-hospitalized persons with symptomatic SARS-CoV-2 infection (NCT04518410). Participants were randomized to receive either bamlanivimab or placebo, with frequent NP swab and daily anterior nasal (AN) swab collection. We utilized quantitative viral load testing and Spike (S) gene next-generation sequencing to assess the emergence of viral resistance mutations to bamlanivimab and their impact on viral load (VL) dynamics. These results provide a window into the dynamic nature of SARS-CoV-2 intrahost viral population shifts and demonstrate that in non-immunosuppressed persons, the emergence of viral resistance against single mAb treatment can alter viral decay kinetics and lead to loss of antiviral activity.

Results

SARS-CoV-2 resistance mutations emerging with mAb treatment were associated with changes in viral replication kinetics

A total of 94 participants were enrolled in the 7,000 mg cohort (48 in the treatment arm and 46 in the placebo arm, enrolled between August 2020 and October 2020) and 223 participants were enrolled in the ACTIV-2/A5401 phase 2 bamlanivimab 700 mg cohort (111 in the treatment and 112 in placebo arms, enrolled between October 2020 and November

2020). The 7,000 mg dosing group was halted before reaching the enrolment goal of 220 participants due to the results of the BLAZE-1 study showing similar reductions in respiratory tract viral load between the bamlanivimab 7,000 mg and 700 mg groups⁹. Viral sequences were successfully obtained from 207 participants in the 700 mg bamlanivimab study and 78 participants in the 7,000 mg study, from at least 1 respiratory sample with quantitative SARS-CoV-2 measurement $\geq 2 \log_{10}$ RNA copies per ml at baseline or during 28 days of follow-up. Sequences were successfully obtained from 96% (729/759) of samples sequenced in the 700 mg group and 98% (244/250) of samples sequenced in the 7,000 mg group, with most failures being among samples with viral loads of 2–3 \log_{10} RNA copies per ml. Primary resistance mutations (L452R, E484K, E484Q, F490S and S494P)^{7,12} at $\geq 20\%$ frequency were not detected in any participants in the 7,000 mg bamlanivimab study, either at baseline or following the single infusion. In the 700 mg bamlanivimab arm, three participants had primary resistance mutations at baseline (one L452R in the setting of B.1.427/429/Epsilon variant infection and two participants with E484K), while the placebo arm had two cases of resistance mutations present at baseline (both L452R in the setting of Epsilon infection, Fig. 1). Treatment-emergent mutations at $\geq 20\%$ frequency (not detected at baseline) were significantly more likely to be detected after bamlanivimab 700 mg treatment than the placebo (7% vs 0%, *P* = 0.003); E484K was found in 5 of 8 cases of emergent resistance, E484Q in two cases and S494P in one case (Fig. 1b). There were two cases of emerging resistance mutations present only as low-frequency variants (<20% frequency): one participant in the placebo arm had an emergent F490S mutation (participant B2_9, Extended Data Fig. 1), while one participant in the bamlanivimab 700 mg treatment arm had emerging S494P concurrent with an emerging E484K (participant B2_6, Extended Data Fig. 1). Among those with emerging resistance,

Table 1 | Demographic characteristics of enrolled participants receiving bamlanivimab treatment, comparing those with emerging resistance to those without any detected resistance mutations

| Characteristic | 7,000 mg treatment w/ bamlanivimab (N=48) | 700 mg treatment w/ bamlanivimab (no resistance) (N=101) | 700 mg treatment w/ bamlanivimab (emerging resistance) (N=8) | P value (comparison between those with and without resistance) |
|--|---|--|--|--|
| Age, median years (Q1, Q3) | 46 (33, 58) | 45 (34, 54) | 56 (50, 64) | 0.01 |
| Female sex, % | 54 | 50 | 50 | 1.0 |
| Race/ethnicity, % | | | | |
| White | 56 | 85 | 75 | 0.61 |
| Black | 6 | 10 | 25 | 0.21 |
| Hispanic | 31 | 17 | 13 | 1.0 |
| Other | 6 | 5 | 0 | 1.0 |
| BMI, median score (Q1, Q3) | 28.2 (24.8, 31.8) | 28.2 (25.1, 33.7) | 29.4 (26.4, 38.2) | 0.36 |
| Baseline NP VL, median log ₁₀ SARS-CoV-2 copies per ml (Q1, Q3) | 5.2 (2.4, 6.6) | 5.5 (3.9, 6.8) | 7.6 (6.4, 8.0) | 0.04 |
| Baseline AN VL, median log ₁₀ SARS-CoV-2 copies per ml (Q1, Q3) | 4.1 (1.0, 5.9) | 4.3 (2.3, 6.1) | 6.6 (5.8, 7.3) | 0.02 |
| Days from symptom onset to randomization, median days (Q1, Q3) | 6.0 (4.0, 8.0) | 6.0 (5.0, 8.0) | 4.5 (2.5, 7.5) | 0.15 |
| Baseline total symptom score, median score (Q1, Q3) | 8.0 (5.0, 10.0) | 9.0 (6.0, 12.0) | 9.0 (5.0, 14.8) | 0.90 |

One participant had both baseline and emerging resistance and was included in the emerging resistance category. Statistical analysis was performed using Mann-Whitney *U* tests for continuous variables and Fisher's exact tests for discrete variables. BMI, body mass index.

only one participant (participant B2_7) had documented immunosuppression, having rheumatoid arthritis being treated with a regimen of methotrexate (2.5 mg) and dexamethasone (6 mg).

Quantitative SARS-CoV-2 viral loads were measured from NP swabs at days 0, 3, 7, 14, 21 and 28 of the trial, and from AN swabs daily at each of the first 14 days and at days 21 and 28. We assessed differences in viral loads in those receiving bamlanivimab 700 mg treatment by the presence of emerging resistance. Pretreatment NP and AN swab viral loads were higher for participants with emerging resistance mutations compared to those with no mutations (emerging vs no mutation viral loads at day 0, NP swab: median 7.6 vs 5.5 log₁₀ copies per ml, *P* = 0.04; AN swab: median 6.6 vs 4.3 log₁₀ copies per ml, *P* = 0.02, Table 1). Those with emerging resistance also had persistently elevated NP and AN viral loads throughout the first 14 days after study enrolment (Fig. 2). Individuals with emerging resistance were older (emerging vs no mutation: median age 56 vs 45 years, *P* = 0.01) and while not statistically significant, the median duration of symptoms at study entry was modestly shorter in those with emerging resistance compared with those without any mutations (emerging vs no mutations: median 4.5 vs 6.0 days, Table 1). Six of the participants with emerging resistance had samples available for baseline serologies and all were negative for IgG antibodies (Extended Data Fig. 2). Measurements of bamlanivimab serum concentrations in participants with emerging resistance showed results generally concordant with expected values for the 700 mg dose, including for maximal concentrations (*C*_{max}) at the end of infusion and concentrations at day 28 (Supplementary Table 1)¹³. One participant (B2_6) had a serum concentration at day 28 below the limit of quantitation and an elimination half-life faster than typical.

Evidence of dynamic SARS-CoV-2 viral population shifts and differential viral fitness after mAb treatment

We observed that the emergence of SARS-CoV-2 resistance mutations was closely associated with a relatively consistent change in viral load kinetics. This is exemplified in Fig. 3 with two examples of viral rebound in participants with emergence of escape variants. In case B2_3, intensive S gene sequencing of virus isolated from the AN swabs revealed the emergence of the E484K resistance mutation on study day 3 as a

low-frequency variant that rapidly took over as the majority population by the next day (Fig. 3a, lower panel) and was associated with a 3.6 log₁₀ increase in AN swab viral loads over the subsequent 4 days to a peak of 7.8 log₁₀ copies per ml on study day 7 before declining. For B2_2, the participant had evidence of baseline E484K mutation and low-frequency E484Q in the NP swab (Fig. 3b). The AN swab showed low-frequency E484K and Q mutations. After bamlanivimab treatment, there were rapid, dynamic shifts in the viral population in the AN swab sample including both the E484K and Q mutations, with the viral load peaking at 6.8 log₁₀ copies per ml over 8 days concurrent with E484Q becoming the dominant mutation. Among the 8 participants with emerging resistance, the median AN swab viral load increase was 3.3 (range 0.3–5.2) log₁₀ RNA copies per ml over a median of 4.5 days (Extended Data Fig. 1) and this viral rebound is highlighted in the comparison of median viral loads between those with and without emerging resistance mutations (Fig. 2).

To quantify the replicative fitness of the different strains, we developed a mathematical model and fit it to both viral load data and variant frequency data collected from 6 participants in the treatment arm with either E484K or Q resistance emergence. In this model, we assumed that each variant is initially present and grows or declines exponentially at a constant rate (see Methods) as was consistent with the data (Extended Data Fig. 3). We chose the first 8–13 timepoints for model fitting, covering the emergence of the resistance mutations but before the eventual viral load declines. We estimated both the initial viral load and the rate of exponential increase or decrease for each variant. From the estimation across the 6 individuals, the wild-type amino acid (that is, 484E) always declined under treatment, with the exponential rate varying from –0.2 to –3.2 per day (Supplementary Table 2). In contrast, the mutant 484K always increased under mAb treatment, confirming it was a resistant mutant, with an exponential growth rate that varied over a wide range (0.5–2.3 per day, Extended Data Fig. 3g). The 484Q mutant was found in two participants, including low-frequency E484K and Q present at baseline in the AN swab sample of participant B2_2. We estimated that virus harbouring 484Q was more fit than 484K in the setting of antibody treatment and grew at approximately twice the rate of the 484K variant (Supplementary Table 2). In participant B2_5, viral

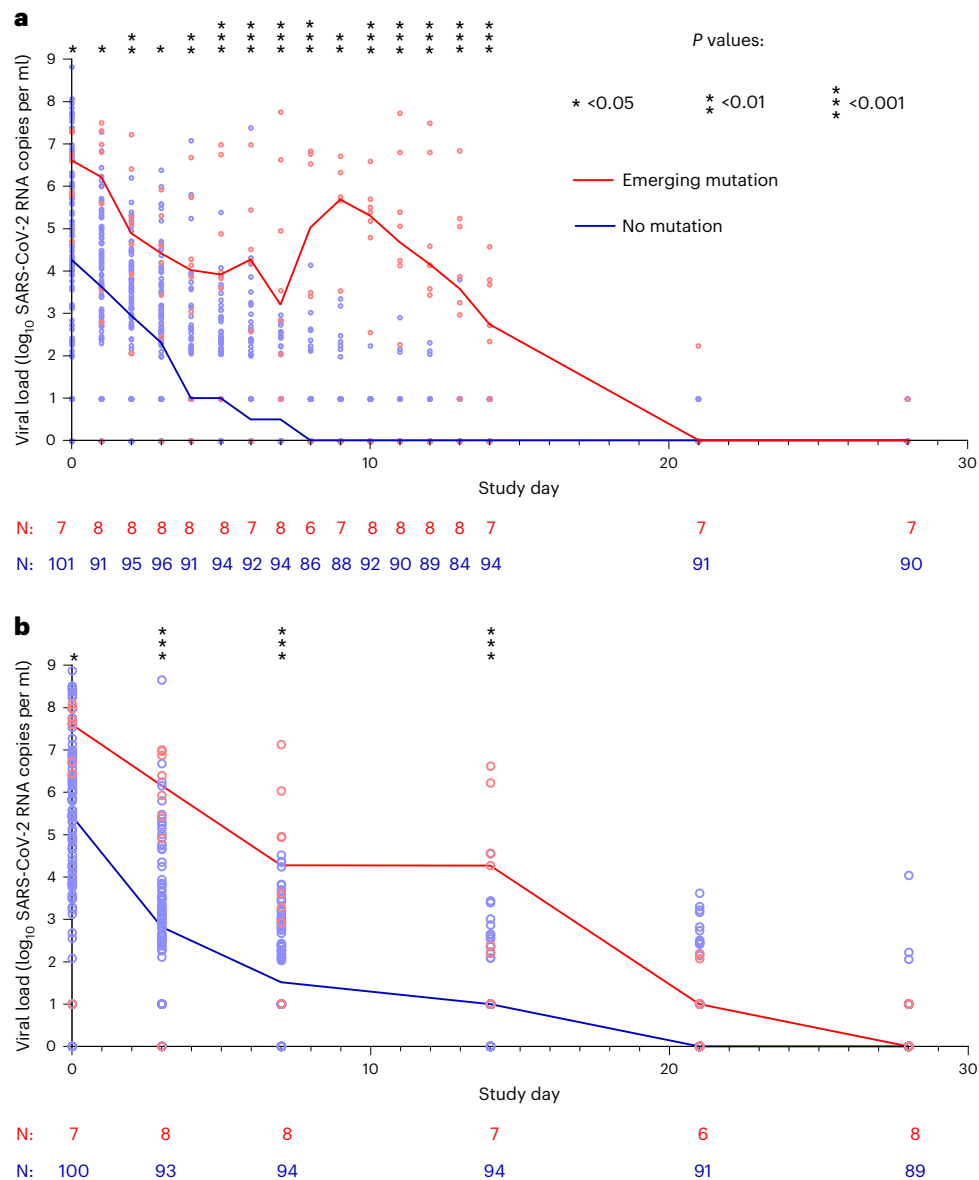


Fig. 2 | SARS-CoV-2 viral kinetics in the bamlanivimab 700 mg treatment arm. a,b, SARS-CoV-2 viral loads from NP swabs collected at days 0, 3, 7, 14, 21 and 28 (a) and from AN swabs collected daily through day 14 followed by days 21 and 28 (b) plotted against study day. Lines show median viral load. The lower limit of quantification was 2.0 \log_{10} SARS-CoV-2 RNA copies per ml, while the lower limit of detection was 1.0 \log_{10} copies per ml. Viral loads between groups were

compared at each timepoint using two-sided Mann-Whitney *U* tests, denoted by asterisks wherever significant. NP day 0 $P = 0.0369$, NP days 3, 7, 14 $P < 0.001$, AN day 0 $P = 0.0135$, AN day 1 $P = 0.0402$, AN day 2 $P = 0.0066$, AN day 3 $P = 0.0145$, AN day 4 $P = 0.0013$, AN days 5–8 $P < 0.001$, AN day 9 $P = 0.0018$, AN days 10–14 $P < 0.001$).

loads in the setting of the 484Q mutant declined, but with a rate much slower than the wild-type 484E, suggesting that it is more fit than 484E in the presence of the mAb or developing host immune responses.

Emergence of additional Spike polymorphisms

In those with emerging bamlanivimab resistance, we next assessed the emergence of additional S gene sequence changes outside of the primary sites of resistance (L452R, E484K, E484Q, F490S and S494P). We found that emergence of additional polymorphisms was common and could be detected in all participants with either baseline or emerging bamlanivimab primary resistance mutations, although most were present at low frequencies (Fig. 4). One emergent polymorphism, Q493R, was detected in B2_7 and has been described as a potential bamlanivimab resistance site¹⁰. Interestingly, a number of polymorphisms were detected at sites distinct from the bamlanivimab site of

activity and probably reflect escape from host immune pressures. For example, deletions at amino acid (AA) positions 141–143 were detected to emerge in both participants B2_2 and B2_4. These N-terminal domain (NTD) deletions have previously been described in immunosuppressed participants with immune escape and persistent COVID-19^{14,15}. These deletions have also been detected in the wider pandemic and represent a common site of viral escape against antibody pressure on the NTD¹⁶. A number of emerging polymorphisms were also detected that are also in several variants of concern and postulated to be involved in either immune escape or enhanced receptor binding. These include L5F (PID B2_2, also in B.1.526/Iota), P9L (PID B2_2, also in C.1.2), L18F (PID B2_8, also in B.1.351/Beta, P.1/Gamma), D138Y (in P.1/Gamma), N501Y (ACE-2 binding domain mutation in PID B2_10, also in B.1.1.7/Alpha, B.1.351/Beta, P.1/Gamma) and P681H (furin cleavage site mutation in PID B2_10, also in B.1.1.7/Alpha)^{17,18}.

We used day 7 NP swab sequencing results to compare the rate of polymorphism emergence across the participant groups as AN swab sequencing was performed only for participants with evidence of resistance emergence. We detected no significant differences in the number of emerging polymorphisms between those with emerging resistance, treated participants without resistance and participants who received the placebo (Extended Data Fig. 4).

Viral rebound after bamlanivimab resistance emergence is associated with worsened symptoms

To assess the clinical relevance of the resurgence in viral loads seen in patients with emerging bamlanivimab resistance mutations, we estimated longitudinal total symptom scores that are based on a 28-day diary completed by the study participants for 13 targeted symptoms¹⁹ and compared these for bamlanivimab-treated participants with and without emerging resistance mutations. On an individual-level, higher symptom scores were frequently reported after the emergence of resistance-associated mutations, as well as increases in respiratory tract viral loads (Fig. 5a). In the population analysis, no significant differences in symptom scores between groups were seen before the emergence of resistance mutations. In participants of the bamlanivimab 700 mg treatment arm with emerging resistance mutations, median AN viral load increase began at the time of resistance detection, with significantly higher subsequent viral loads and total symptom scores compared with those in the treatment arm without resistance (Fig. 5b). All participants, regardless of study arm or resistance status, resolved their symptoms by study day 28.

Discussion

In this analysis of a randomized placebo-controlled clinical trial of non-hospitalized persons with early COVID-19, we report the emergence of resistance mutations to the mAb bamlanivimab and the effects of these mutations on viral decay and clinical symptoms. These results represent the clearest evidence so far of several key principles: (1) the dynamic nature of SARS-CoV-2 evolution and replication during mAb treatment, (2) treatment-emergent SARS-CoV-2 resistance mutations alter viral replication kinetics and extend the period of high viral loads, (3) emerging mAb resistance mutations can lead to increased viral shedding from the respiratory tract and resurgent symptoms and (4) the emergence of resistance to mAb treatment may be dependent on the treatment dose.

In immunocompromised persons with COVID-19, viral evolution can lead to immune escape and rapid emergence against even combination mAb therapy^{11,15,20,21}. Whether these findings are generalizable to the immunocompetent population has been unclear and there has not been definitive evidence that the emergence of SARS-CoV-2 escape mutations impacts in vivo viral replication dynamics and loss of therapeutic efficacy. In this study of bamlanivimab in a general population of outpatients with mild to moderate COVID-19, we show that resistance mutations to monoclonal antibody treatment can emerge quickly and are associated with rapid and sustained increase in respiratory tract SARS-CoV-2 viral load. This increase in viral load correlated with worsened self-reported clinical symptoms over the subsequent days, although symptoms eventually resolved by study day 28. These results are consistent with previous reports that during acute SARS-CoV-2 infection, high-level respiratory tract viral loads often precede symptom onset by 1–2 days²².

One limitation of this phase 2 study is the limited sample size, especially in the bamlanivimab 7,000 mg cohort. While treatment-emergent mutations were not found in ACTIV-2 participants receiving the higher 7,000 mg dose of bamlanivimab, they were frequently detected in the larger BLAZE-1 phase 2 trial of the 7,000 mg dose⁷. One difference between these studies was the longer duration of symptoms before the start of treatment for the ACTIV-2 participants who enrolled a median of 6 days since symptom onset versus 4 days for the BLAZE-1 participants.

This probably led to higher pretreatment viral loads in the BLAZE-1 study, which we found to be a risk factor for resistance emergence. Unfortunately, baseline viral loads could not be compared between studies as the BLAZE-1 study did not use a quantitative SARS-CoV-2 viral load assay. These disparate results highlight the importance of incorporating quantitative viral load testing and resistance testing for COVID-19 treatment trials of mAbs and other antiviral agents.

Monoclonal antibody efficacy, including bamlanivimab, appears to wax and wane depending on the dominant variant¹³. Within this evolving landscape, this study acts as an informative model system for illustrating the interplay between mAb resistance mutations, viral kinetics and symptoms. The richness of the dataset, derived from logistically intense daily respiratory sampling, has not been reported before and will be challenging to replicate. With the emergence of the Omicron variant, it is more important than ever to understand this relationship, especially as we are again relying on single effective mAbs, such as bebtelovimab²³ for treatment and prevention. While bebtelovimab is effective across a broad range of variants, early phase clinical studies have demonstrated a similar level of emerging resistance as in bamlanivimab²³, and we believe our data may also provide insight into virologic and clinical characteristics of treatment failure for other single mAb treatments.

We were able to identify several potential factors that may increase or decrease the risk of mAb resistance. We found that older age and higher baseline respiratory tract viral load were associated with higher risk of resistance emergence, while none of the 48 participants treated with the higher 7,000 mg bamlanivimab dose developed resistance. Studies of mAb treatments have suggested that earlier initiation of therapy during periods of high respiratory tract viral load is associated with a greater reduction in respiratory tract viral load and probably improved therapeutic efficacy²⁴. Our data suggest that mAb treatment during periods of high-level viral loads may come at the cost of increased risk of resistance emergence, although this effect may be mitigated by using higher doses of mAbs or potentially combination mAb therapy. Interestingly, we also noted frequent increase in viral loads associated with resistance emergence that lasted several days to more than a week before declining. Such prolonged rise in viral loads is unusual, especially as these individuals had a median of 5 days of symptoms by the time of study entry and it is expected that levels of respiratory viral loads should already be declining²⁵. While the exact cause is unclear, this finding raises several intriguing possibilities. First, antiviral mAb therapies may have host immune modulating effects beyond their capacity to bind and neutralize viral particles²⁶. It is unknown whether mAb therapeutics may in some cases interfere with host immune responses, especially in the setting of mAb resistance, leading to suboptimal viral control. Alternatively, there have also been reports from in vitro studies that certain SARS-CoV-2-specific antibodies may lead to antibody-dependent enhancement of infection through an Fcγ receptor-dependent mechanism²⁷, particularly at sub-neutralizing concentrations, although in vivo confirmation has been challenging to obtain.

Our study also found that SARS-CoV-2 populations can turn over quickly, allowing for quick selection of drug resistance-associated mutations against single mAb treatment. In fact, viral populations were found to be able to completely shift from fully sensitive to fully resistant viruses within 24 hours. The emerging primary resistance mutations (for example, E484K/Q) described in this report not only confer resistance to mAb therapy but can also lead to decreased efficacy of vaccine-induced immune responses²⁸. While the rate of total polymorphism accumulation did not appear to be higher in those who developed bamlanivimab resistance, many of the emerging polymorphisms are also key mutations found in several variants of concern/interest (including B.1.1.7/Alpha, B.1.351/Beta and P.1/Gamma), which are associated with increased transmission efficiency and enhanced outbreaks²⁹. The impact of treatment-induced resistance mutations on the spread of these key escape mutations should be further assessed.

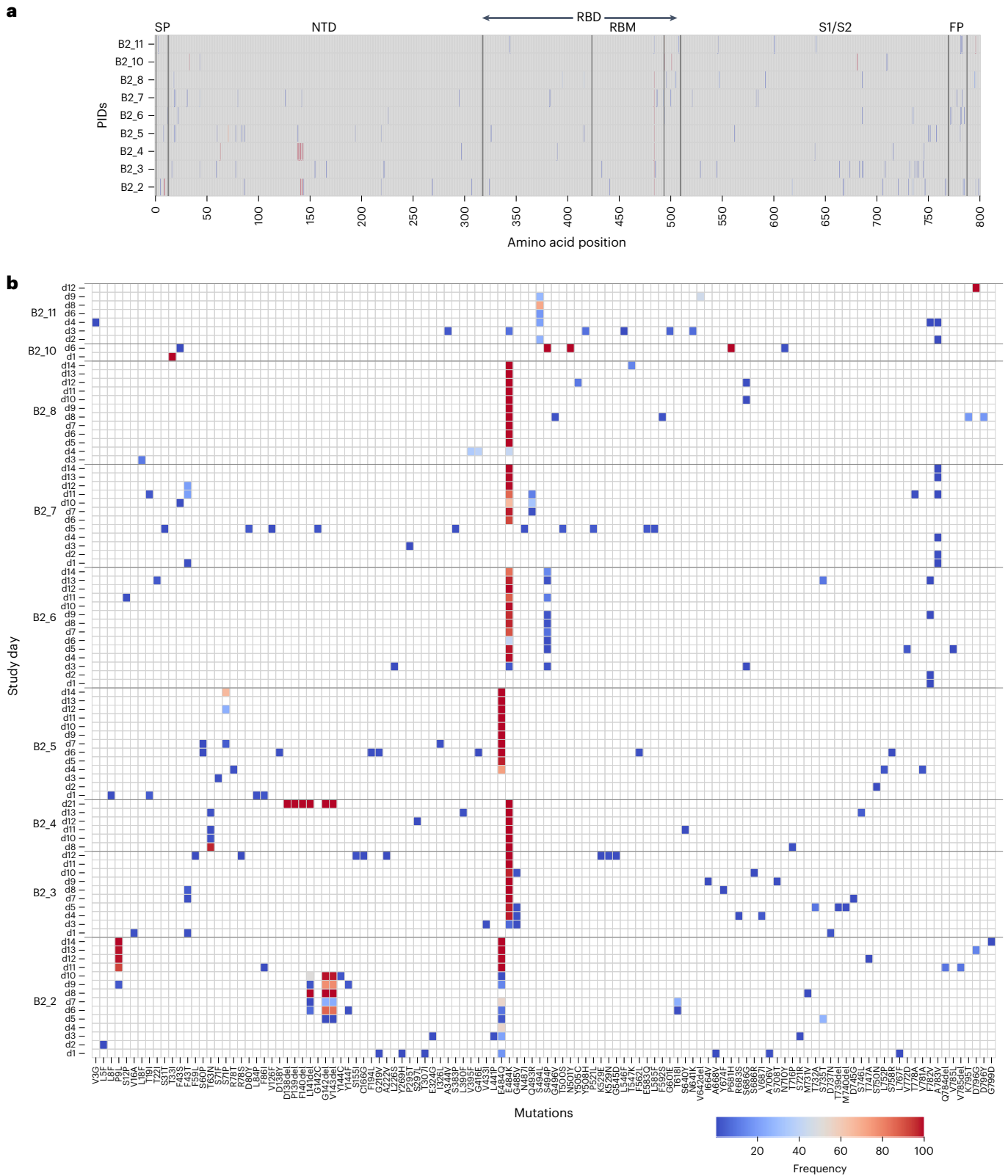


Fig. 4 | Heat map showing distribution of Spike polymorphisms from AN swab samples in bamlanivimab 700 mg treated participants with emerging primary resistance mutations. a, Polymorphism in the context of near-full length Spike gene. Y axis shows participants' ID (PID) followed by day of sample collection, while x axis shows amino acid positions in the Spike gene. Different domains of Spike are shown at the top. **b**, Zoomed-in heat map showing sites that harbour polymorphisms in at least one of the samples across different

participants. Colours indicate frequency of polymorphisms, with blue indicating the lowest value and red indicating the highest value in the scale. The order of samples is the same as that in **a**. The x axis denotes amino acid sites, with number indicating position of amino acids, and letters before and after the numbers indicating wild-type and polymorphic amino acid, respectively. SP, signal peptide; RBM, receptor binding motif.

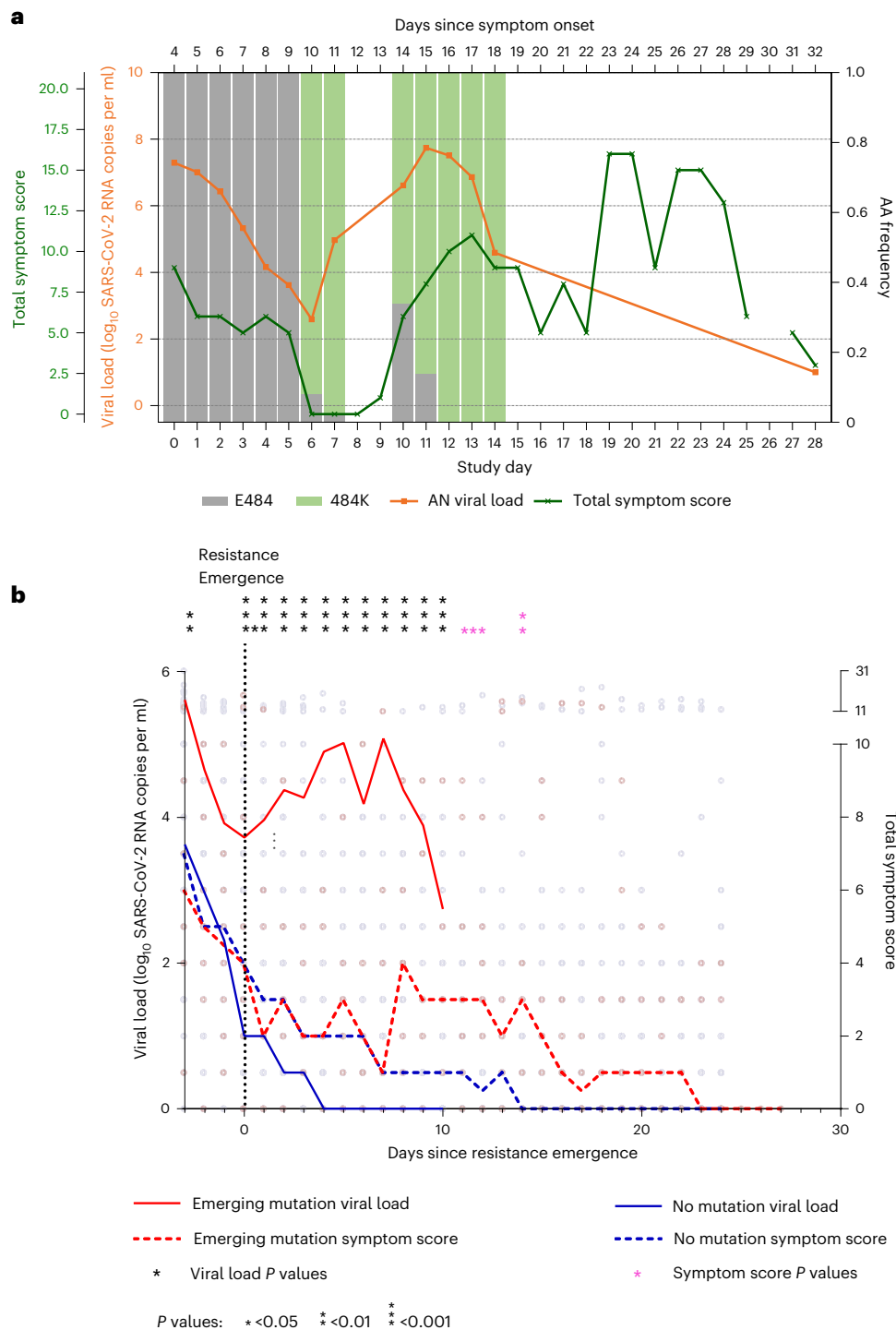


Fig. 5 | Worsened COVID-19 symptoms with viral resurgence after emergence of resistance mutations. **a**, Example of increased AN viral load and total symptom score (TSS) trend for one participant, B2_7, with emerging E484K resistance after bamlanivimab 700 mg treatment. **b**, Median AN viral load (solid line) and total symptom score (dashed line) plotted from the days since symptom emergence (DSSE) to $\geq 20\%$ of the viral population (day 0) for participants in the bamlanivimab 700 mg treatment group with (red) and without (green) emerging

resistance mutations. For participants without emerging resistance, day 0 was equivalent to study day 4, which represented the median day of resistance emergence for those with emerging resistance. AN viral load and TSS between the emerging resistance and no emerging resistance groups were compared at each day by two-sided Mann-Whitney *U* tests: VL: -3 DSSE $P = 0.0054$, -1 DSSE $P = 0.0325$, 0-10 DSSE $P < 0.001$; TSS: 11 DSSE $P = 0.0368$, 12 DSSE $P = 0.0339$, 14 DSSE $P = 0.056$, 15 DSSE $P = 0.0240$.

In summary, these results provide clear evidence that single mAb treatment can rapidly select for SARS-CoV-2 resistance in immunocompetent patients in vivo, leading to viral rebound and correlating with worsened self-reported symptom severity. While initiation of

mAb treatment during early infection is recommended for optimal therapeutic benefit, our results suggest that emerging resistance is a potential risk with single mAb treatment during periods of high-level viral replication. These findings have implications for the design and

utilization of SARS-CoV-2 antiviral therapeutics and provide insights into the prevention of SARS-CoV-2 resistance. Careful assessment of viral dynamics and resistance in response to new treatments for COVID-19 should be prioritized.

Methods

Study participants and sample collection

The study participants were enrolled in the ACTIV-2/AIDS Clinical Trials Group (ACTG) A5401 phase 2 randomized, placebo-controlled trial of bamlanivimab 7,000 mg and 700 mg mAb therapy (NCT04518410) (Chew et al.). The protocol was approved by a central institutional review board (IRB), Advarra (Pro00045266), with additional local IRB review and approval as required by participating sites. All participants provided written informed consent. Participant compensation varied by site and was approved before participant accrual by central and/or local IRBs and ethical committees, as required for each site. Symptomatic adults ≥ 18 years of age with a documented positive SARS-CoV-2 antigen or nucleic acid test and without the need for hospitalization were enrolled if the diagnostic sample was collected ≤ 7 days before study entry and within 10 days of symptom onset. The 7,000 mg dosing group was halted early due to the results of the BLAZE-1 study showing similar virologic efficacy between the bamlanivimab 7,000 mg and 700 mg groups⁹. A total of 95 and 222 participants were randomized in the bamlanivimab 7,000 mg and the 700 mg study, respectively, and received an intervention (one bamlanivimab or placebo intravenous infusion). NP swab samples were collected by research staff at study days 0, 3, 7, 14 and 28, while AN swabs were self-collected by participants daily through study day 14 and at days 21 and 28. Swabs were placed in 3 ml of media (RPMI with 2% FBS).

Total symptom scores were calculated on the basis of a 28 day diary completed by the participants for 13 targeted symptoms¹⁹. The targeted symptoms are feeling feverish, cough, shortness of breath or difficulty breathing, sore throat, body pain or muscle pain or aches, fatigue, headache, chills, nasal obstruction or congestion, nasal discharge, nausea, vomiting and diarrhoea. Each symptom is scored daily by the participant as absent (score 0), mild (1), moderate (2) and severe (3).

SARS-CoV-2 VL testing and S gene next-generation sequencing

SARS-CoV-2 viral loads from NP and AN swab samples were quantified using the Abbott m2000 system. SARS-CoV-2 quantitative Laboratory Developed Test (LDT) was developed utilizing open-mode functionality on m2000sp/rt (Abbott) using EUA Abbott SARS-CoV-2 qualitative reagents³⁰. Identical extraction and amplification protocols developed for RealTime SARS-CoV-2 qualitative EUA assay were also used for the development of the RealTime SARS-CoV-2 quantitative LDT³¹. In this assay, 2 calibrator levels (3 log₁₀ RNA copies per ml and 6 log₁₀ RNA copies per ml) tested in triplicate were used to generate a calibration curve, and 3 control levels (negative, low positive at 3 log₁₀ RNA copies per ml and high positive at 5 log₁₀ RNA copies per ml) were included in each run for quality management. In addition, batches of a matrix-specific control ('external' swab control) with a target of 200 copies per ml were prepared and one unit was included in every run. All controls were monitored using Levy-Jennings plots to monitor inter-run precision. Specimens that were greater than 7 log₁₀ RNA copies per ml were diluted 1:1,000 and rerun to obtain an accurate viral load result. The lower limit of quantification was 2.0 log₁₀ SARS-CoV-2 RNA copies per ml.

S gene sequencing was performed on NP swab samples at two timepoints for all participants: baseline (study entry) and the last sample with VL ≥ 2 log₁₀ SARS-CoV-2 RNA copies per ml. In participants with evidence of slow viral decay (VL ≥ 2 log₁₀ copies per ml at study day 14) or viral rebound (increase in NP swab VL), we performed S gene sequencing of all NP swab samples with VL ≥ 2 log₁₀ copies per ml. Sequencing of daily AN swab samples was performed for participants with any emerging bamlanivimab resistance mutations detected on NP swab samples. Viral RNA extraction was performed on 1 ml of

swab fluid using the TRIzol-LS reagent (ThermoFisher) as previously described³². Complementary DNA synthesis was performed using Superscript IV reverse transcriptase (Invitrogen) following the manufacturer's instructions. Spike gene amplification was performed using a nested PCR strategy with *in-house* designed primer sets targeting codons 1–814 of the Spike. PCR products were pooled, and Illumina library construction was performed using the Nextera XT library prep kit (Illumina). Sequencing was performed on the Illumina MiSeq platform. Raw sequence data were analysed using PASEq v1.4 (<https://www.paseq.org>). Briefly, data were quality filtered using Trimmomatic (v0.30), with a Q25/5 bp sliding window and a 70 bp minimum length. Non-viral contamination was filtered out using BBSplit v35.76. Filtered reads were then merged with pear v0.9.6 aligned to the reference sequence using Bowtie2 (v2.1.0). Amino acid variants were then called at the codon level using perl code and used for resistance interpretation with a 1% limit of detection.

Detection of Spike mutations

We assessed the presence of previously confirmed bamlanivimab resistance mutations (L452R, E484K, E484Q, F490S and S494P)^{7,12}. The detection of resistance mutations down to 1% frequency was performed using PASEq³³. Mutations detected by next-generation sequencing at $< 20\%$ of the viral population were labelled as 'low-frequency' variants as they would largely be missed by traditional Sanger sequencing. A minimum average of 500x sequencing coverage per sample was required for variant calling.

Serology

IgG antibodies recognizing SARS-CoV-2 Spike, RBD, Nucleocapsid (N) and NTD proteins were measured in serum samples using a commercially available multiplex kit (K15359U, Meso Scale Diagnostics). Assays were performed according to kit instructions. Briefly, plates were treated with MSD blocker A to prevent non-specific antibody binding. Serum samples were thawed and diluted 1:500 and 1:5,000 in MSD diluent. IgG was detected by incubation with MSD SULFO-TAG anti-IgG antibody. Measurements were performed with a MESO Quickplex SQ 120 reader. Three internal serum controls provided by MSD were run with each plate. Pre-pandemic sera from healthy adult donors ($n = 10$; AMSBIO, 02141) were included as additional negative controls for the assays. Threshold values for antibody titre (Spike, RBD and N proteins) were provided by MSD and were based on analyses of 200 pre-2019 and 214 COVID + (PCR-confirmed) COVID-19 patients. The thresholds utilized provide 84%, 71% and 71% sensitivity and 99.5%, 98.5% and 100% specificity for Spike, RBD and N antibody responses, respectively. NTD thresholds were not available.

Pharmacokinetic analysis

Blood samples for quantitation of bamlanivimab serum concentrations were collected pre-dose and at the following times after the end of infusion: 30 min, days 14 and 28, and weeks 12 and 24. Pharmacokinetic parameters of interest were maximum concentration (C_{max}), elimination half-life and clearance (CL), and were calculated on the basis of the statistical moment theory using the trapezoidal rule and linear regression (WinNonLin, Certara).

Statistical analysis and mathematical modelling

The non-parametric Mann-Whitney U test was used to compare differences in viral loads between groups. Chi-squared tests and Fisher's exact tests were used for analyses of proportions. All statistical analyses were performed in GraphPad Prism (version 9.1.1). Intensive AN swab viral loads and sequences were used for mathematical modelling. The mutational load was calculated by multiplying resistance mutation frequency by the total viral load. In the model, we assumed that the i th variant, V_i , has an initial load $V_{i,0}$ and its population size changes exponentially at a constant rate, r_i :

$$V_i(t) = V_{i,0}e^{r_i t}.$$

Then, the total viral load at time t , $V(t)$ was calculated as:

$$V(t) = \sum_i V_{i,0}e^{r_i t}.$$

The model-predicted frequency of each variant was

$$f_i(t) = \frac{V_{i,0}e^{r_i t}}{V(t)}.$$

We estimated the initial load, $V_{i,0}$ and the rate of exponential increase/decrease, r_i , from the viral load and viral frequency data fitted simultaneously. Note that in this model, we assumed that the observed mutants were present at the time of antibody infusion or were produced quickly near that time.

To calculate the goodness of fit of the model to the data, we first calculated the residual sum of squares (RSS) between the model-predicted viral load and the measured viral load on a logarithmic scale using \log_{10} . The log-scale was used because viral loads were measured using PCR and the measurement error was thus multiplicative, making the logarithm the natural scale to use. We then calculated the RSS between model-predicted frequencies and measured frequencies for the mutants. The final RSS was calculated as the sum of the two RSS errors:

$$\text{RSS} = \sum_k \left[(\log_{10} V(t_k) - \log_{10} Y_k)^2 + \sum_i (f_i(t_k) - F_{i,k})^2 \right]$$

where k denotes the k^{th} timepoint, Y_k and $F_{i,k}$ respectively denote the measured viral load and the measured frequency for the i^{th} variant at the k^{th} timepoint. Parameter values were estimated by minimizing the RSS using the built-in 'Nelder-Mead' method of the `optim` function in the R programming language (<http://www.r-project.org/>).

Reporting summary

Further information on research design is available in the Nature Research Reporting Summary linked to this article.

Data availability

The authors confirm that all data underlying the findings are fully available. Due to ethical restrictions, study data are available upon request at <https://submit.mis.s-3.net/>, and will require the written agreement of the AIDS Clinical Trials Group and the manufacturer of the investigational product. Completion of an ACTG Data Use Agreement may be required. Source data are provided with this paper. The next-generation sequencing data generated in this study have been deposited on the NCBI Short Read Archive (SRA) under accession number [PRJNA816433](https://www.ncbi.nlm.nih.gov/submit/sra/#?term=PRJNA816433) and [PRJNA859660](https://www.ncbi.nlm.nih.gov/submit/sra/#?term=PRJNA859660).

Code availability

Code used for mathematical modelling is available from the corresponding authors upon request.

References

- Moore, C. B. et al. Evidence of HIV-1 adaptation to HLA-restricted immune responses at a population level. *Science* **296**, 1439–1443 (2002).
- Plant, E. P., Manukyan, H., Sanchez, J. L., Laassri, M. & Ye, Z. Immune pressure on polymorphous influenza b populations results in diverse hemagglutinin escape mutants and lineage switching. *Vaccines* <https://doi.org/10.3390/vaccines8010125> (2020).
- Larder, B. A. & Kemp, S. D. Multiple mutations in HIV-1 reverse transcriptase confer high-level resistance to zidovudine (AZT). *Science* **246**, 1155–1158 (1989).
- Chou, S., Guentzel, S., Michels, K. R., Miner, R. C. & Drew, W. L. Frequency of UL97 phosphotransferase mutations related to ganciclovir resistance in clinical cytomegalovirus isolates. *J. Infect. Dis.* **172**, 239–242 (1995).
- Takashita, E. et al. Global update on the susceptibilities of human influenza viruses to neuraminidase inhibitors and the cap-dependent endonuclease inhibitor baloxavir, 2017–2018. *Antivir. Res.* **175**, 104718 (2020).
- Clavel, F. & Hance, A. J. HIV drug resistance. *N. Engl. J. Med.* **350**, 1023–1035 (2004).
- Gottlieb, R. L. et al. Effect of bamlanivimab as monotherapy or in combination with etesevimab on viral load in patients with mild to moderate COVID-19: a randomized clinical trial. *JAMA* **325**, 632–644 (2021).
- Fact Sheet for Health Care Providers: Emergency Use Authorization (EUA) of Casirivimab and Imdevimab* (FDA, accessed 31 October 2021); <https://www.fda.gov/media/145611/download>
- Chen, P. et al. SARS-CoV-2 neutralizing antibody LY-CoV555 in outpatients with Covid-19. *N. Engl. J. Med.* **384**, 229–237 (2021).
- Starr, T. N., Greaney, A. J., Dingens, A. S. & Bloom, J. D. Complete map of SARS-CoV-2 RBD mutations that escape the monoclonal antibody LY-CoV555 and its cocktail with LY-CoV016. *Cell Rep. Med.* **2**, 100255 (2021).
- Starr, T. N. et al. Prospective mapping of viral mutations that escape antibodies used to treat COVID-19. *Science* **371**, 850–854 (2021).
- McCallum, M. et al. SARS-CoV-2 immune evasion by the B.1.427/B.1.429 variant of concern. *Science* <https://doi.org/10.1126/science.abi7994> (2021).
- Fact Sheet for Health Care Providers: Emergency Use Authorization (EUA) of Bamlanivimab and Etesevimab* (FDA, accessed 14 July 2021); <https://www.fda.gov/media/145802/download>
- Truong, T. T. et al. Increased viral variants in children and young adults with impaired humoral immunity and persistent SARS-CoV-2 infection: a consecutive case series. *EBioMedicine* **67**, 103355 (2021).
- Choi, B. et al. Persistence and evolution of SARS-CoV-2 in an immunocompromised host. *N. Engl. J. Med.* **383**, 2291–2293 (2020).
- McCarthy, K. R. et al. Recurrent deletions in the SARS-CoV-2 spike glycoprotein drive antibody escape. *Science* **371**, 1139–1142 (2021).
- Luan, B., Wang, H. & Huynh, T. Enhanced binding of the N501Y-mutated SARS-CoV-2 spike protein to the human ACE2 receptor: insights from molecular dynamics simulations. *FEBS Lett.* **595**, 1454–1461 (2021).
- Gupta, R. K. Will SARS-CoV-2 variants of concern affect the promise of vaccines. *Nat. Rev. Immunol.* **21**, 340–341 (2021).
- Chew, K. W. et al. Antiviral and clinical activity of bamlanivimab in a randomized trial of non-hospitalized adults with COVID-19. *Nat. Commun.* **13**, 4931 (2022).
- Ko, S. H. et al. High-throughput, single-copy sequencing reveals SARS-CoV-2 spike variants coincident with mounting humoral immunity during acute COVID-19. *PLoS Pathog.* **17**, e1009431 (2021).
- Choudhary, M. C., Crain, C. R., Qiu, X., Hanage, W. & Li, J. Z. SARS-CoV-2 sequence characteristics of COVID-19 persistence and reinfection. *Clin. Infect. Dis.* <https://doi.org/10.1093/cid/ciab380> (2021).
- He, X. et al. Temporal dynamics in viral shedding and transmissibility of COVID-19. *Nat. Med.* <https://doi.org/10.1038/s41591-020-0869-5> (2020).
- Fact Sheet for Healthcare Providers: Emergency Use Authorization for Bebtelovimab* (FDA, accessed 16 April 2022); <https://www.fda.gov/media/156152/download>

24. Weinreich, D. M. et al. REGN-COV2, a neutralizing antibody cocktail, in outpatients with Covid-19. *N. Engl. J. Med.* **384**, 238–251 (2021).
25. Wolfel, R. et al. Virological assessment of hospitalized patients with COVID-2019. *Nature* <https://doi.org/10.1038/s41586-020-2196-x> (2020).
26. Pelegrin, M., Naranjo-Gomez, M. & Piechaczyk, M. Antiviral monoclonal antibodies: can they be more than simple neutralizing agents? *Trends Microbiol.* **23**, 653–665 (2015).
27. Zhou, Y. et al. Enhancement versus neutralization by SARS-CoV-2 antibodies from a convalescent donor associates with distinct epitopes on the RBD. *Cell Rep.* **34**, 108699 (2021).
28. Collier, D. A. et al. Sensitivity of SARS-CoV-2 B.1.1.7 to mRNA vaccine-elicited antibodies. *Nature* **593**, 136–141 (2021).
29. Campbell, F. et al. Increased transmissibility and global spread of SARS-CoV-2 variants of concern as at June 2021. *Euro Surveill.* <https://doi.org/10.2807/1560-7917.ES.2021.26.24.2100509> (2021).
30. Degli-Angeli, E. et al. Validation and verification of the Abbott RealTime SARS-CoV-2 assay analytical and clinical performance. *J. Clin. Virol.* **129**, 104474 (2020).
31. Berg, M. G. et al. Development of the RealTime SARS-CoV-2 quantitative laboratory developed test and correlation with viral culture as a measure of infectivity. *J. Clin. Virol.* **143**, 104945 (2021).
32. Fajnzylber, J. et al. SARS-CoV-2 viral load is associated with increased disease severity and mortality. *Nat. Commun.* **11**, 5493 (2020).
33. Lee, E. R. et al. Performance comparison of next generation sequencing analysis pipelines for HIV-1 drug resistance testing. *Sci. Rep.* **10**, 1634 (2020).

Acknowledgements

We thank the participants, site staff, site investigators and the entire ACTIV-2/A5401 study team. We also thank the PASEq team (R. Paredes and M. Noguera Julian) for their support.

This work was supported by the National Institute of Allergy and Infectious Diseases of the National Institutes of Health under Award Number 3UM1AI068636-14S2, UM1 AI068634, UM1 AI068636 and UM1 AI106701. The content is solely the responsibility of the authors and does not necessarily represent the official views of the National Institutes of Health. Portions of this work were done under the auspices of the US Department of Energy under contract 89233218CNA000001 and supported by NIH grants R01-OD011095 and R01-AI028433 (ASP), R01-AI116868 (RMR) and R01-AI152703 and U54-HL143541 (RK).

Author contributions

M.C.C., K.W.C., D.M.S. and J.Z.L. conceptualized and performed the study; M.C.C., R.D., J.P.F., J. Regan and C.R.C. performed resistance analysis experiments; R.M.R., R.K. and A.S.P. performed mathematical modelling; J.A.D. and A.L.G. performed viral load analysis; U.M.P. and S.F.S. performed serological analysis; C.M., M.D.H. and J. Ritz

performed statistical analysis; A.C.J. A.N., P.K., E.S.D, D.A.W., J.J.E, J.S.C., R.W.C. helped in manuscript writing and in providing critical input; C.V.F. performed pharmacokinetic analysis.

Competing interests

KWC received research funding to the institution from Merck Sharp & Dohme and is a consultant for Pardes Biosciences. ESD receives consulting fees from Gilead Sciences, Merck and GSK/ViiV and research support through the institution from Gilead Sciences and GSK/ViiV. DAW received funding to the institution to support research and honoraria for advisory boards and consulting from Gilead Sciences. JZL has consulted for Abbvie. C. ALG reports contract testing from Abbott and research support from Merck and Gilead. PK and AN are employees and shareholders of Eli Lilly. JJE is an ad hoc consultant to GSK/VIR, data monitoring committee (DMC) chair for Adagio Phase III studies. JSC has consulted for Merck and Company. DMS consulted for the following companies Fluxergy, Kiadis, Linear Therapies, Matrix BioMed, Arena Pharmaceuticals, VxBiosciences, Model Medicines, Bayer Pharmaceuticals, Signant Health and Brio Clinical. PK and AN are employees and shareholders of Eli Lilly. All other authors (MCC, RD, JPF, JRegan, CRC, MDH, JRitz, RMR, RK, JAD, ACJ, CVF, UMP, SFS, ASP, RWC) report no competing interests.

Additional information

Extended data is available for this paper at <https://doi.org/10.1038/s41564-022-01254-1>.

Supplementary information The online version contains supplementary material available at <https://doi.org/10.1038/s41564-022-01254-1>.

Correspondence and requests for materials should be addressed to Davey M. Smith or Jonathan Z. Li.

Peer review information *Nature Microbiology* thanks the anonymous reviewers for their contribution to the peer review of this work.

Reprints and permissions information is available at www.nature.com/reprints.

Publisher's note Springer Nature remains neutral with regard to jurisdictional claims in published maps and institutional affiliations.

Springer Nature or its licensor holds exclusive rights to this article under a publishing agreement with the author(s) or other rightsholder(s); author self-archiving of the accepted manuscript version of this article is solely governed by the terms of such publishing agreement and applicable law.

© The Author(s), under exclusive licence to Springer Nature Limited 2022

Manish C. Choudhary^{1,3,33}, **Kara W. Chew**^{2,3,33}, **Rinki Deo**¹, **James P. Flynn**¹, **James Regan**¹, **Charles R. Crain**¹, **Carlee Moser**³, **Michael D. Hughes**³, **Justin Ritz**³, **Ruy M. Ribeiro**⁴, **Ruian Ke**⁴, **Joan A. Dragavon**⁵, **Arzhang Cyrus Javan**⁶, **Ajay Nirula**⁷, **Paul Klekotka**⁷, **Alexander L. Greninger**⁵, **Courtney V. Fletcher**⁸, **Eric S. Daar**⁹, **David A. Wohl**¹⁰, **Joseph J. Eron**¹⁰, **Judith S. Currier**¹⁰, **Urvi M. Parikh**¹¹, **Scott F. Sieg**¹², **Alan S. Perelson**⁴, **Robert W. Coombs**⁵, **Davey M. Smith**^{13,33} ✉, **Jonathan Z. Li**^{1,3,33} ✉ and for the **ACTIV-2/A5401 Study Team***

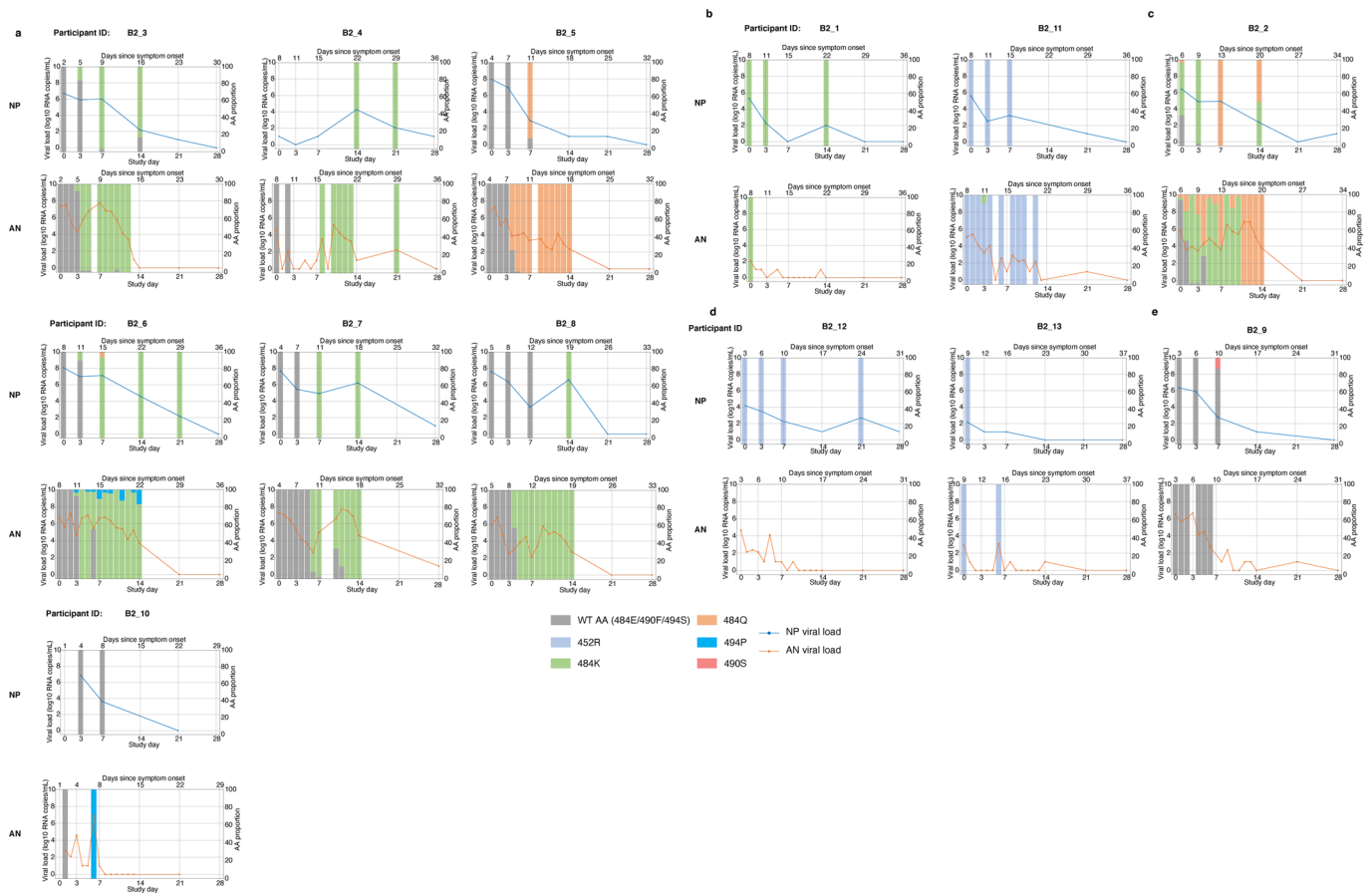
¹Department of Medicine, Division of Infectious Diseases, Brigham and Women's Hospital, Harvard Medical School, Boston, MA, USA. ²Department of Medicine, David Geffen School of Medicine, University of California, Los Angeles, CA, USA. ³Harvard T.H. Chan School of Public Health, Boston, MA, USA. ⁴Theoretical Biology and Biophysics Group, Los Alamos National Laboratory, Los Alamos, NM, USA. ⁵Department of Laboratory Medicine and Pathology,

University of Washington, Seattle, WA, USA. ⁶National Institutes of Health, Bethesda, MD, USA. ⁷Lilly Research Laboratories, San Diego, CA, USA. ⁸Center for Drug Discovery, University of Nebraska Medical Center, Omaha, NE, USA. ⁹Lundquist Institute at Harbor-UCLA Medical Center, Torrance, CA, USA. ¹⁰Department of Medicine, University of North Carolina at Chapel Hill School of Medicine, Chapel Hill, NC, USA. ¹¹Division of Infectious Diseases, University of Pittsburgh School of Medicine, Pittsburgh, PA, USA. ¹²Department of Medicine, Division of Infectious Diseases and HIV Medicine, Case Western Reserve University, Cleveland, OH, USA. ¹³Department of Medicine, University of California, San Diego, CA, USA. ³³These authors contributed equally: Manish C. Choudhary, Kara W. Chew, Davey M. Smith, Jonathan Z. Li. *A list of authors and their affiliations appears at the end of the paper. ✉e-mail: davey@ucsd.edu; jli@bwh.harvard.edu

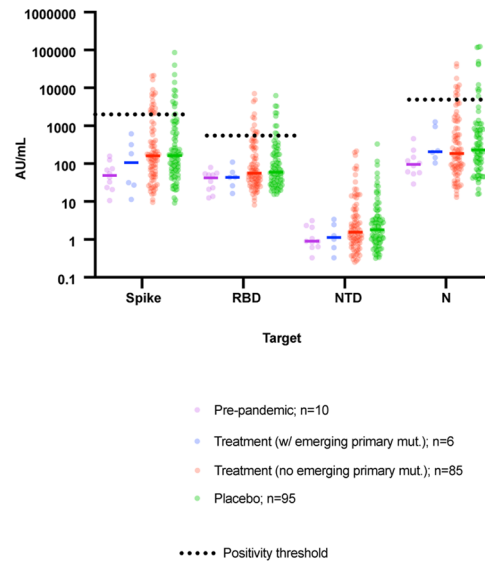
for the ACTIV-2/A5401 Study Team

Kara W. Chew^{2,33}, David (Davey) Smith¹³, Eric S. Daar⁹, David A. Wohl¹⁰, Judith S. Currier², Joseph J. Eron¹⁰, Arzhang Cyrus Javan¹⁴, Michael D. Hughes³, Carlee Moser³, Mark Giganti³, Justin Ritz³, Lara Hosey¹⁵, Jhoanna Roa¹⁵, Nilam Patel¹⁵, Kelly Colsh¹⁶, Irene Rwakazina¹⁶, Justine Beck¹⁶, Scott Sieg¹⁷, Jonathan Z. Li^{1,33}, Courtney V. Fletcher⁸, William Fischer¹⁰, Teresa Evering¹⁸, Rachel Bender Ignacio¹⁹, Sandra Cardoso²⁰, Katya Corado⁹, Prasanna Jagannathan²¹, Nikolaus Jilg²², Alan S. Perelson⁴, Sandy Pillay²³, Cynthia Riviere²⁴, Upinder Singh²¹, Babafemi Taiwo²⁵, Joan Gottesman²⁶, Matthew Newell¹⁰, Susan Pedersen¹⁰, Joan Dragavon⁵, Cheryl Jennings²⁷, Brian Greenfelder²⁸, William Murtaugh²⁹, Jan Kosmyna³⁰, Morgan Gapara^{31,32}, Akbar Shahkolahi¹⁵ and Paul Klekotka⁷

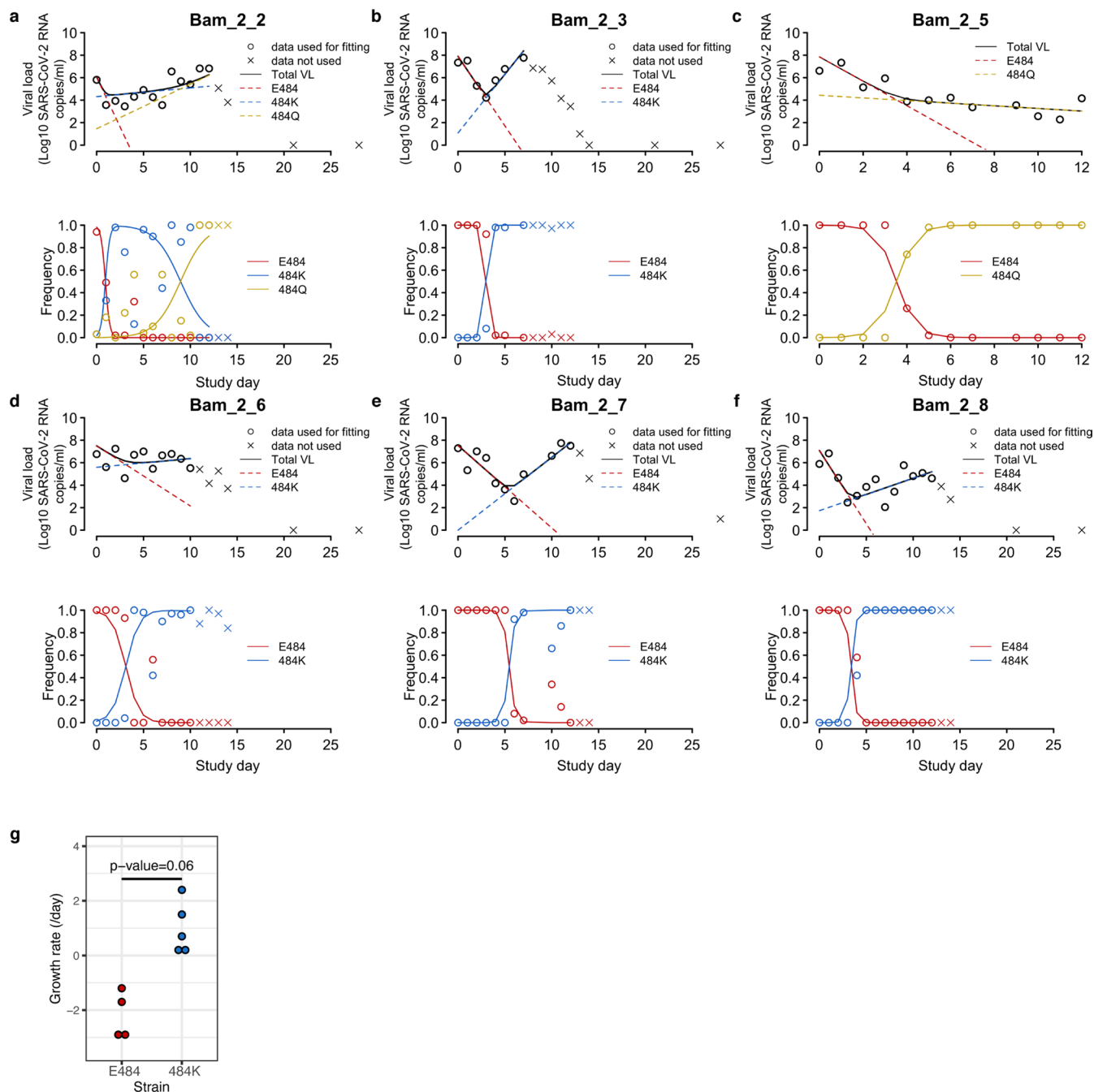
¹⁴NIH Division of AIDS (DAIDS), National Institutes of Health, Rockville, MD, USA. ¹⁵AIDS Clinical Trials Group (ACTG) Network Coordinating Center, Social and Scientific Systems, a DLH Company, Silver Spring, MD, USA. ¹⁶NIH/DAIDS Pharmaceutical Affairs Branch, Rockville, MD, USA. ¹⁷Case Western Reserve University, Cleveland, OH, USA. ¹⁸Weill Cornell Medicine, New York, NY, USA. ¹⁹University of Washington, Seattle, WA, USA. ²⁰Fundação Oswaldo Cruz, Rio de Janeiro, Brazil. ²¹Stanford University School of Medicine, Palo Alto, CA, USA. ²²Massachusetts General Hospital, Harvard Medical School, Boston, MA, USA. ²³Enhancing Care Foundation, Durban, KwaZulu-Natal, South Africa. ²⁴GHESKIO Center, Port-au-Prince, Haiti. ²⁵Northwestern University Feinberg School of Medicine, Chicago, IL, USA. ²⁶Vanderbilt University Medical Center, Nashville, TN, USA. ²⁷Northwestern University, Chicago, IL, USA. ²⁸Ohio State University, Columbus, OH, USA. ²⁹ACTG Laboratory Center, University of California, Los Angeles, CA, USA. ³⁰ACTG Community Scientific Subcommittee, Case Western University Clinical Research Site, North Royalton, OH, USA. ³¹ACTG Network Coordinating Center, Social and Scientific Systems, a DLH Company, Durham, NC, USA. ³²Los Alamos National Laboratory, Los Alamos, NM, USA.



Extended Data Fig. 1 | Viral load and primary resistance mutation frequencies. Viral loads and frequencies of primary resistance mutations from nasopharyngeal swab (NP) and anterior nasal swab (AN) samples for participants displaying primary bamlanivimab resistance mutations.

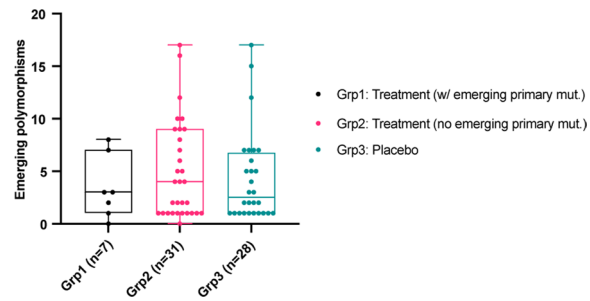


Extended Data Fig. 2 | SARS-CoV-2 specific IgG antibody profiling at baseline in different study groups. SARS-CoV-2 specific IgG antibody profiling at baseline in different study groups. Horizontal bars represent median antibody titer. Dashed lines represent antibody positivity detection threshold. RBD denotes Receptor binding domain, NTD N-terminal domain, N Nucleocapsid.



Extended Data Fig. 3 | Fitting of the mathematical model to viral load and viral frequency data in individuals with resistance mutations. Fitting of the mathematical model to viral load and viral frequency data in individuals with resistance mutations. (A-F) In each panel, the upper plot shows the viral load kinetics in the individual with the ID shown in the title; the lower plot shows the frequencies over time for the mutants under analysis. Data used for model fitting

are shown as 'o' and data not used for model fitting are shown as 'x'. Simulation results using the best-fit parameters (Supplemental Table 2) are shown as lines. (G) Comparison of growth rates of the E484 and the 484 K strains estimated from mathematical models for 5 individuals. P-value is calculated using a Wilcoxon signed rank test for paired data.



Extended Data Fig. 4 | Emerging polymorphisms in different participant counts. Emerging polymorphisms in different participant counts. Counts of emerging polymorphisms (including primary resistance sites) in NP samples on day 7 in three study groups: participants with emerging primary resistance

mutations, treatment group participants without emerging primary resistance mutations, and the placebo group. Box plots show median and interquartile range.

Reporting Summary

Nature Portfolio wishes to improve the reproducibility of the work that we publish. This form provides structure for consistency and transparency in reporting. For further information on Nature Portfolio policies, see our [Editorial Policies](#) and the [Editorial Policy Checklist](#).

Statistics

For all statistical analyses, confirm that the following items are present in the figure legend, table legend, main text, or Methods section.

- | | |
|-------------------------------------|--|
| n/a | Confirmed |
| <input type="checkbox"/> | <input checked="" type="checkbox"/> The exact sample size (n) for each experimental group/condition, given as a discrete number and unit of measurement |
| <input type="checkbox"/> | <input checked="" type="checkbox"/> A statement on whether measurements were taken from distinct samples or whether the same sample was measured repeatedly |
| <input type="checkbox"/> | <input checked="" type="checkbox"/> The statistical test(s) used AND whether they are one- or two-sided <i>Only common tests should be described solely by name; describe more complex techniques in the Methods section.</i> |
| <input type="checkbox"/> | <input checked="" type="checkbox"/> A description of all covariates tested |
| <input type="checkbox"/> | <input checked="" type="checkbox"/> A description of any assumptions or corrections, such as tests of normality and adjustment for multiple comparisons |
| <input type="checkbox"/> | <input checked="" type="checkbox"/> A full description of the statistical parameters including central tendency (e.g. means) or other basic estimates (e.g. regression coefficient) AND variation (e.g. standard deviation) or associated estimates of uncertainty (e.g. confidence intervals) |
| <input type="checkbox"/> | <input checked="" type="checkbox"/> For null hypothesis testing, the test statistic (e.g. F , t , r) with confidence intervals, effect sizes, degrees of freedom and P value noted <i>Give P values as exact values whenever suitable.</i> |
| <input checked="" type="checkbox"/> | <input type="checkbox"/> For Bayesian analysis, information on the choice of priors and Markov chain Monte Carlo settings |
| <input checked="" type="checkbox"/> | <input type="checkbox"/> For hierarchical and complex designs, identification of the appropriate level for tests and full reporting of outcomes |
| <input checked="" type="checkbox"/> | <input type="checkbox"/> Estimates of effect sizes (e.g. Cohen's d , Pearson's r), indicating how they were calculated |

Our web collection on [statistics for biologists](#) contains articles on many of the points above.

Software and code

Policy information about [availability of computer code](#)

- | | |
|-----------------|--|
| Data collection | No software was used for data collection. |
| Data analysis | Statistical analysis was performed using GraphPad Prism 9.1.1. The following software was used for sequence assembly and minority variant analysis: PaSeq v1.4 (paseq.org), Trimmomatic v0.30, BBSplit v35.76, pear v0.9.6, and Bowtie2 v2.1.0. Pharmacokinetic parameter estimation was performed using WinNonLin. Mathematical modeling of resistance mutant fitness was performed using the R programming language. |

For manuscripts utilizing custom algorithms or software that are central to the research but not yet described in published literature, software must be made available to editors and reviewers. We strongly encourage code deposition in a community repository (e.g. GitHub). See the Nature Portfolio [guidelines for submitting code & software](#) for further information.

Data

Policy information about [availability of data](#)

All manuscripts must include a [data availability statement](#). This statement should provide the following information, where applicable:

- Accession codes, unique identifiers, or web links for publicly available datasets
- A description of any restrictions on data availability
- For clinical datasets or third party data, please ensure that the statement adheres to our [policy](#)

The authors confirm that all data underlying the findings are fully available. Due to ethical restrictions, study data are available upon request from sdac.data@sdac.harvard.edu with the written agreement of the AIDS Clinical Trials Group and the manufacturer of the investigational product.

Field-specific reporting

Please select the one below that is the best fit for your research. If you are not sure, read the appropriate sections before making your selection.

Life sciences Behavioural & social sciences Ecological, evolutionary & environmental sciences

For a reference copy of the document with all sections, see [nature.com/documents/nr-reporting-summary-flat.pdf](https://www.nature.com/documents/nr-reporting-summary-flat.pdf)

Life sciences study design

All studies must disclose on these points even when the disclosure is negative.

| | |
|-----------------|---|
| Sample size | The current study includes all participants of the phase 2 bamlanivimab protocol of A5401/ACTIV-2. Sample size determination is detailed in the study protocol, which is included as a supplement to this manuscript. |
| Data exclusions | <i>Describe any data exclusions. If no data were excluded from the analyses, state so OR if data were excluded, describe the exclusions and the rationale behind them, indicating whether exclusion criteria were pre-established.</i> |
| Replication | Sequencing and viral load results from respiratory samples were confirmed through sampling both nasopharyngeal swabs and anterior nasal swabs. Serum samples were run in duplicate for detection of IgG antibodies. The quantitative viral load assay is EUA authorized and passed all external proficiency testing. All attempts at replication were successful. |
| Randomization | The 7000mg treatment group was enrolled first, followed by the 700mg treatment group. After enrollment, participants were randomly assigned by a web-based interactive response system in a 1:1 ratio to receive either bamlanivimab or placebo. Randomization was stratified by time from symptom onset (\leq or $>$ 5 days) and risk of progression to severe COVID-19 ("higher" vs "lower"). "Higher" risk was defined in the protocol as meeting any of the following: age \geq 55 years or having a comorbidity (chronic lung disease or moderate to severe asthma, body mass index $>$ 35 kg/m ² , hypertension, cardiovascular disease, diabetes, or chronic kidney or liver disease). |
| Blinding | Investigators were blinded during the sample collection and assay performance. |

Reporting for specific materials, systems and methods

We require information from authors about some types of materials, experimental systems and methods used in many studies. Here, indicate whether each material, system or method listed is relevant to your study. If you are not sure if a list item applies to your research, read the appropriate section before selecting a response.

Materials & experimental systems

| n/a | Involved in the study |
|-------------------------------------|---|
| <input type="checkbox"/> | <input checked="" type="checkbox"/> Antibodies |
| <input checked="" type="checkbox"/> | <input type="checkbox"/> Eukaryotic cell lines |
| <input checked="" type="checkbox"/> | <input type="checkbox"/> Palaeontology and archaeology |
| <input checked="" type="checkbox"/> | <input type="checkbox"/> Animals and other organisms |
| <input type="checkbox"/> | <input checked="" type="checkbox"/> Human research participants |
| <input type="checkbox"/> | <input checked="" type="checkbox"/> Clinical data |
| <input checked="" type="checkbox"/> | <input type="checkbox"/> Dual use research of concern |

Methods

| n/a | Involved in the study |
|-------------------------------------|---|
| <input checked="" type="checkbox"/> | <input type="checkbox"/> ChIP-seq |
| <input checked="" type="checkbox"/> | <input type="checkbox"/> Flow cytometry |
| <input checked="" type="checkbox"/> | <input type="checkbox"/> MRI-based neuroimaging |

Antibodies

| | |
|-----------------|---|
| Antibodies used | The MSD SULFO-TAG anti-Human IgG antibody (Meso Scale Diagnostics, Rockville, MD; catalog # K15359U) was used to detect anti-SARS-CoV-2 spike, receptor binding domain, N-terminal domain, and nucleocapsid IgG. MSD SULFO-TAG anti-IgG antibody is provided as a 200X stock solution that is diluted to a 1X solution. |
| Validation | <p>The MSD SULFO-TAG anti-Human IgG was reported by the manufacturer (Meso Scale Diagnostics, Rockville, MD) to be validated for use in their V-Plex SARS-CoV-2 serology panels (catalog # K15359U).</p> <p>Serology reference standard 1 for assay calibration and three control serums consisting of specific concentrations of human IgG recognizing antigens in the multiplex assay (lot-specific certifications at www.msd.com) are provided with the MSD kit.</p> <p>References using this technology:</p> <p>Immunogenicity of Ad26.COV2.S vaccine against SARS-CoV-2 variants in humans Galit Alter, Jingyou Yu, Jinyan Liu, Abishek Chandrashekar, Erica N Borducchi, Lisa H Tostanoski, Katherine McMahan, Catherine Jacob-Dolan, David R Martinez, Aiquan Chang, Tochi Anioke, Michelle Lifton, Joseph Nkolola, Kathryn E Stephenson, Caroline Atyeo, Sally Shin, Paul Fields, Ian Kaplan, Harlan Robins, Fatima Amanat, Florian Krammer, Ralph S Baric, Mathieu Le Gars, Jerald Sadoff, Anne Marit de Groot, Dirk Heerwegh, Frank Struyf, Macaya Douoguih, Johan van Hoof, Hanneke Schuitemaker, Dan H Barouch</p> |

Evaluation of a novel multiplexed assay for determining IgG levels and functional activity to SARS-CoV-2
 Marina Johnson, Helen R. Wagstaffe, Kimberly C. Gilmour, Annabelle Lea Mai, Joanna Lewis, Adam Hunt, Jake Sirr, Christopher Bengt, Louis Grandjean, David Goldblatt
 Journal of Clinical Virology
 2020
 Nature
 2021

Two doses of SARS-CoV-2 vaccination induce robust immune responses to emerging SARS-CoV-2 variants of concern
 Donal T. Skelly, Adam C. Harding, Javier Gilbert-Jaramillo, Michael L. Knight, Stephanie Longet, Anthony Brown, Sandra Adele, Emily Adland, Helen Brown, Medawar Laboratory Team, Tom Tipton, Lizzie Stafford, Alexander J. Mentzer, Sile A. Johnson, Ali Amini, OPTIC (Oxford Protective T cell Immunology for COVID-19) Clinical Group, Tiong Kit Tan, Lisa Schimanski, Kuan-Ying A. Huang, Pramila Rijal, PITCH (Protective Immunity T cells in Health Care Worker) Study Group, C-MORE/PHOSP-C Group, John Frater, Philip Goulder, Christopher P. Conlon, Katie Jeffery, Christina Dold, Andrew J. Pollard, Alex Sigal, Tulio de Oliveira, Alain R. Townsend, Paul Klenerman, Susanna J. Dunachie, Eleanor Barnes, Miles W. Carroll & William S. James

Coronavirus-Specific Antibody Cross Reactivity in Rhesus Macaques Following SARS-CoV-2 Vaccination and Infection
 Catherine Jacob-Dolan, Jared Feldman, Katherine McMahan, Jingyou Yu, Roland Zahn, Frank Wegmann, Hanneke Schuitemaker, Aaron G Schmidt, Dan H Barouch
 Journal of Virology
 2021

Immunogenicity of Ad26.COV2.S vaccine against SARS-CoV-2 variants in humans
 Galit Alter, Jingyou Yu, Jinyan Liu, Abishek Chandrashekar, Erica N Borducchi, Lisa H Tostanoski, Katherine McMahan, Catherine Jacob-Dolan, David R Martinez, Aiquan Chang, Tochi Anioke, Michelle Lifton, Joseph Nkolola, Kathryn E Stephenson, Caroline Atyeo, Sally Shin, Paul Fields, Ian Kaplan, Harlan Robins, Fatima Amanat, Florian Krammer, Ralph S Baric, Mathieu Le Gars, Jerald Sadoff, Anne Marit de Groot, Dirk Heerwegh, Frank Struyf, Macaya Douoguih, Johan van Hoof, Hanneke Schuitemaker, Dan H Barouch
 Nature
 2021
 Nature Communications
 2021

Human research participants

Policy information about [studies involving human research participants](#)

Population characteristics

Participant characteristics are described in Table 1.

Recruitment

Participants were recruited through a variety of mechanisms including a study-specific website with IRB-approved content describing the study. The website listed a telephone number that connected to a 24 hour call center staffed by English and Spanish speaking operators who followed an IRB-approved script to pre-screen callers for basic eligibility (e.g., recent diagnosis of COVID-19, age of 18 and older) and then connected callers to the nearest study site. In addition, digital marketing was conducted using the paid search services of the Google search engine such that IRB-approved advertisements for the trial were displayed when searching key words (e.g., COVID-19 treatment, COVID-19 treatment trial). IRB-approved study advertisements were also placed periodically on Facebook and Instagram. Persons testing COVID-19 positive at testing venues associated with the clinical laboratories Covance and Quest, operated by eTrueNorth Inc, or partnered with Verily Life Sciences or the PPD Accelerated Enrollment Solutions (AES) and who opted-in to receive information regarding research opportunities received IRB-approved messages or calls describing the study. Study sites also conducted their own outreach including the circulation of IRB-approved brochures, postcards, and flyers at COVID-19 testing centers. Lastly, the trial was listed on the NIH-operated public access website www.clinicaltrials.gov. Participant compensation varied by site and was approved prior to participant accrual by central and/or local IRBs and ECs, as required for each site.

Ethics oversight

Study protocol approval and ethical oversight was performed by a central Institutional Review Board (Advarra, Inc.).

Note that full information on the approval of the study protocol must also be provided in the manuscript.

Clinical data

Policy information about [clinical studies](#)

All manuscripts should comply with the ICMJE [guidelines for publication of clinical research](#) and a completed [CONSORT checklist](#) must be included with all submissions.

Clinical trial registration

NCT04518410

Study protocol

The study protocol is provided as a supplement to this manuscript.

Data collection

Participants were enrolled and data was collected at multiple sites within in the United States. A full list of participating sites and investigators is included as a supplement to this manuscript. 94 participants were enrolled in the 7000mg cohort between August 2020 and October 2020, and 223 participants were enrolled in the 700mg cohort between October 2020 and November 2020. Respiratory sampling was performed up to 28 days after study entry. Blood draws for serological profiling were performed at study entry as well as 28 days and 12 weeks after study entry.

Outcomes

This paper is reporting on two of the trial's exploratory outcomes: to explore baseline and emergent viral resistance to the investigational agent and to explore the association between viral genotypes and phenotypes, and clinical outcomes and response to agents. These measures were assessed through targeted S gene next generation sequencing of patient respiratory samples to detect baseline and emergent drug resistance and relating these sequencing results to patient viral loads and symptom scores.